The Astrophysical Journal, 832:172 (9pp), 2016 December 1 doi:10.3847/0004-637X/832/2/172

DIFFUSE AURORA ON GANYMEDE DRIVEN BY ELECTROSTATIC WAVES

R. P. Singhal, A. K. Tripathi[1], S. Halder, and O. N. Singh II
Department of Physics, Indian Institute of Technology (Banaras Hindu University), Varanasi-221005 (UP), India; rpsiitbhu@yahoo.comaktrip2001@yahoo.co.inh. santanu5791@gmail.com, ons_onkaritapd@yahoo.co.in
Received 2016 June 19; revised 2016 September 17; accepted 2016 September 21; published 2016 November 30

ABSTRACT

The role of electrostatic electron cyclotron harmonic (ECH) waves in producing diffuse auroral emission O I 1356 Å on Ganymede is investigated. Electron precipitation flux entering the atmosphere of Ganymede due to pitch-angle diffusion by ECH waves into the atmospheric loss-cone is calculated. The analytical yield spectrum approach for electron energy degradation in gases is used for calculating diffuse auroral intensities. It is found that calculated O I 1356 Å intensity resulting from the precipitation of magnetospheric electrons observed near Ganymede is insufficient to account for the observed diffuse auroral intensity. This is in agreement with estimates made in earlier works. Heating and acceleration of ambient electrons by ECH wave turbulence near the magnetic equator on the field line connecting Ganymede and Jupiter are considered. Two electron distribution functions are used to simulate the heating effect by ECH waves. Use of a Maxwellian distribution with temperature 100 eV can produce about 50–70 Rayleigh O I 1356 Å intensities, and the kappa distribution with characteristic energy 50 eV also gives rise to intensities with similar magnitude. Numerical experiments are performed to study the effect of ECH wave spectral intensity profile, ECH wave amplitude, and temperature/characteristic energy of electron distribution functions on the calculated diffuse auroral intensities. The proposed missions, joint NASA/ESA *Jupiter Icy Moon Explorer* and the present *JUNO* mission to Jupiter, would provide new data to constrain the ECH wave and other physical parameters near Ganymede. These should help confirm the findings of the present study.

Key words: atomic processes – molecular processes – planets and satellites: aurorae – planets and satellites: individual (Ganymede, Jupiter) – planets and satellites: atmospheres

1. INTRODUCTION

Ganymede is the largest moon of Jupiter and is also the largest moon in the solar system. It has a diameter of 5268 km and orbits Jupiter at distance of 1,070,400 km (~15 R_J, R_J is the radius of Jupiter). Several probes flying by or orbiting Jupiter have explored Ganymede more closely. The first approaches were conducted by the *Pioneer 10* and *11* probes in 1973 and 1974, respectively (Mead 1974). These missions returned information on its physical characteristics and resolved features to 400 km on its surface. The next missions came in 1979, when the *Voyager 1* and *2* probes passed the moon, refining estimates of its size (Gurnett et al. 1979; Scarf et al. 1979). In 1995 the *Galileo* spacecraft orbited Jupiter and went to make six close flybys of Ganymede (G1, G2, G7, G8, G28, and G29) between 1996 and 2000 (Williams et al. 1992; Susanna et al. 2002). The spacecraft had a suite of instruments dedicated to study Jupiter and its satellites. These included the: Plasma Wave Instrument, magnetometer, Energetic Particle Detector, and Plasma Science Experiment. The most recent mission to Ganymede was made by the *New Horizons* probe in 2007 (Grundy et al. 2007) while en route to Pluto. The probe obtained topographic and composition mapping data of Ganymede during its flyby of Jupiter. In addition to these missions, Ganymede has also been studied by the *Hubble Space Telescope* (*HST*).

No atmosphere was revealed on Ganymede by the *Voyager* data. Despite the *Voyager* data, evidence for a tenuous oxygen atmosphere on Ganymede was found from observations by the *HST* in 1995. These observations constrained the fluxes and spectral shapes of the O I 1356 Å and O I 1304 Å emission lines, which imply a molecular oxygen atmosphere with a column density in the range of (1–10) $\times 10^{14}$ cm^{-2} (Hall et al. 1998).

Data from the *Galileo* encounters of Ganymede provided many surprises including the discovery, verification, and initial studies of Ganymede magnetic field, its magnetosphere, its trapped particle populations, and its interaction with the Jovian environment (Gurnett et al. 1996; Kivelson et al. 1996, 1997; Frank et al. 1997; Williams et al. 1997a, 1997b; Williams & Mauk 1997). During the first Ganymede encounter G1, intense plasma waves were detected over a region of nearly four times Ganymede's diameter. The types of waves detected (whistler mode emissions, hybrid waves, electrostatic electron cyclotron waves and escaping radio emission) strongly suggested that Ganymede has an extended magnetosphere of its own. The data indicated the existence of a strong ($B > 400$ nT) magnetic field. Further analysis of data acquired by the *Galileo* magnetometer showed that the permanent dipole moment has an equatorial field magnitude 719 nT (Kivelson et al. 2002). It is tilted by 176° from the spin axis, with the pole in the southern hemisphere rotated by 24° from the Jupiter-facing meridian plane toward the trailing hemisphere.

Ganymede also exhibits auroral emission, first observed by Hall et al. (1998) with the Goddard High Resolution Spectrograph on board the *HST*. The observed double-peaked profile of Ganymede's O I 1356 Å feature indicated a nonuniform spatial emission distribution that suggested two distinct and spatially confined emission regions, consistent with the satellite's north and south poles. Subsequent spatially and spectrally resolved *HST* observations with the Space Telescope Imaging Spectrograph clearly demonstrate the existence of two auroral ovals around Ganymede's magnetic north and south poles as shown in the work of Feldman et al. (2000) and McGrath et al. (2013). Atomic oxygen emission is observed in

[1] Corresponding author.

both hemispheres with maxima at latitudes of about 30°, which is consistent with the magnetic field data—the boundary between Ganymede's open and closed magnetic field lines passes precisely at these latitudes. The aurora brightness data from Feldman et al. (2000) show that there is a background diffuse emission that does not exceed 100 Rayleigh (R) over almost the entire auroral oval region. Localized regions of enhanced emission with an intensity up to 300 R are superimposed on this general background. Auroral emissions result from the interaction of electrons precipitating from the magnetospheric electrons on open field lines with oxygen molecules in Ganymede's tenuous atmosphere. The Jovian magnetospheric plasma at Ganymede is characterized by a thermal component with $n_e \sim 5$–$20\,\mathrm{cm}^{-3}$, $T_e \sim 20\,\mathrm{eV}$, plus a suprathermal component with $n_e \sim 0.5$–$2\,\mathrm{cm}^{-3}$, $T_e \sim 2\,\mathrm{keV}$ (Scudder et al. 1981). The thermal electrons of the Jovian magnetosphere with the above parameters can generate an emission with an intensity of ~10–40 R. In contrast, the observed intensity of 300 R can be achieved only if the electrons are accelerated significantly and are characterized by a Maxwellian distribution with a temperature in the range 75–300 eV (Eviatar et al. 2001). The processes that lead to the acceleration of electrons can be different in nature (Eviatar et al. 2001; Lavrukhin & Alexeev 2015).

It is accepted that the occurrence of diffuse aurora on Earth results from pitch-angle diffusion of electrons into the atmospheric loss-cone due to resonant wave–particle interactions. Plasma waves, considered major candidates responsible for electron scattering, are electrostatic electron cyclotron harmonic (ECH) waves and electromagnetic whistler mode chorus waves. Recent quantitative analyses of the diffuse aurora have demonstrated that whistler mode chorus waves are the dominant scattering mechanism for the diffuse auroral precipitation in the inner magnetosphere at geocentric distances of below ~8 R_E (R_E is the radius of Earth), while ECH waves can act as a major contributor to diffuse auroral precipitation in the outer magnetosphere (Thorne et al. 2010; Ni et al. 2014, 2016).

In the present study we explore the role of electrostatic waves in producing the diffuse emissions on Ganymede. Banded emissions which lie between the harmonics of the electron cyclotron frequency (f_{ce}), often referred to as $(n+1/2)$ f_{ce} emissions or electrostatic ECH emissions, have been observed near Ganymede (Gurnett et al. 1996). Electrostatic ECH waves have also been observed in Jupiter's middle magnetosphere with amplitudes up to a few mV m^{-1} (Gurnett et al. 1979; Scarf et al. 1979; Kurth et al. 1997). ECH waves are driven by an anisotropy in the electron velocity distribution, such as loss-cone anisotropy. A loss-cone anisotropy is produced when particles moving within a cone of directions along the magnetic field (the loss-cone) strike the planet and are lost from the system. Loss-cone distributions are normally associated with radiation belt particles trapped on "closed" magnetic field lines that link the magnetic poles of the same body. However, because Ganymede lies within the magnetosphere of Jupiter, field lines link the magnetic field of Ganymede to the magnetic field of Jupiter. A unique situation arises in which particles are trapped between their Ganymede mirror points and their near Jupiter mirror points. It was suggested by Gurnett et al. (1996) that electron precipitation into Ganymede's atmosphere due to pitch-angle scattering by ECH waves could cause observable optical emissions, possibly accounting for the auroral emissions observed near Ganymede by the *HST* (Calvin et al. 1996). In addition to pitch-angle diffusion, ECH wave turbulence may also heat and accelerate the ambient magnetospheric electrons.

In this work we have used a different, much more comprehensive approach for calculating auroral emissions resulting from energy loss of electrons precipitating into the atmosphere of Ganymede. Numerical experiments have been performed by changing the spectral intensity profile of ECH waves, amplitudes of waves, and energy spectra of precipitating electrons. In Section 2 we present the calculation details. Results are discussed in Section 3 and conclusions of the present study are presented in Section 4.

2. CALCULATION DETAILS

2.1. Precipitation Flux

Electrons will be precipitated into the atmosphere of Ganymede due to pitch-angle diffusion by ECH waves into the atmospheric loss-cone. Precipitation flux ϕ is determined by the differential flux of precipitating electrons inside the equatorial loss-cone (e.g., Chang 1983)

$$\Phi = 2\pi \frac{B_A}{B_{\mathrm{eq}}} \int_{E_1}^{E_2} \int_0^{\alpha_{\mathrm{LC}}} J\,(E_{\mathrm{o}}, \alpha) \cos\alpha \,\sin\alpha \, dE_{\mathrm{o}}\, d\alpha. \quad (1)$$

Here B_{A} is the magnetic field strength at the top of Ganymede's atmosphere, B_{eq} is the field strength at the magnetic equator on the field line connecting Ganymede and Jupiter, J is the electron differential flux inside the equatorial loss-cone (α_{LC}) as a function of energy and pitch angle, and E_1 and E_2 are the lower and upper limit for integration over energy. Equatorial pitch angle α (o to α_{LC}) maps to pitch angle θ_{o} (0 to $\pi/2$) at the top of the atmosphere. The relation between α and θ_{o} is given by

$$\sin^2\alpha / B_{\mathrm{eq}} = \sin^2\theta_{\mathrm{o}} / B_A. \quad (2)$$

Differentiating Equation (2) we obtain

$$\sin\alpha\,\cos\alpha\, B_A / B_{\mathrm{eq}}\, d\alpha = \sin\theta_{\mathrm{o}}\,\cos\theta_{\mathrm{o}}\, d\theta_{\mathrm{o}}. \quad (3)$$

Substituting Equation (3) in Equation (1)

$$\Phi = 2\pi \int_{E_1}^{E_2} \int_0^{\pi/2} J\,(E_{\mathrm{o}}, \alpha(\theta_{\mathrm{o}}))\sin\theta_{\mathrm{o}}\,\cos\theta_{\mathrm{o}}\, dE_{\mathrm{o}}\, d\theta_{\mathrm{o}}, \quad (4)$$

where $\sin\alpha = \sin\theta_{\mathrm{o}}\,\sin\alpha_{\mathrm{LC}}$ and $J(E_{\mathrm{o}}, \alpha)$ is given by (Kennel & Petschek 1966; Ni et al. 2012)

$$J\,(E_{\mathrm{o}}, \alpha(\theta_{\mathrm{o}})) = J\,(E_{\mathrm{o}}, \alpha_{\mathrm{LC}}) \frac{I_{\mathrm{o}}(Z_{\mathrm{o}}\,\alpha/\alpha_{\mathrm{LC}})}{I_{\mathrm{o}}\,(Z_{\mathrm{o}})}, \quad (5)$$

where $Z_{\mathrm{o}} = \sqrt{D_{\mathrm{SD}}/\langle D_{\alpha\alpha}\rangle|_{\alpha_{\mathrm{LC}}}}$, I_{o} is the modified Bessel function of the first kind, and $J\,(E_{\mathrm{o}}, \alpha_{\mathrm{LC}})$ is the electron flux near the equatorial loss-cone. D_{SD} is the strong diffusion rate determined by (Kennel 1969)

$$D_{\mathrm{SD}} = \frac{2\,(\alpha_{\mathrm{LC}})^2}{\tau_B}, \quad (6)$$

τ_B is the electron bounce period along the entire field line. It is set equal to half the bounce time between Jupiter's north and south poles at $L = 15$ (Orlova & Shprits 2011). $\langle D_{\alpha\alpha}\rangle|_{\alpha_{\mathrm{LC}}}$ is the bounce-averaged diffusion coefficient at the edge of the loss-cone.

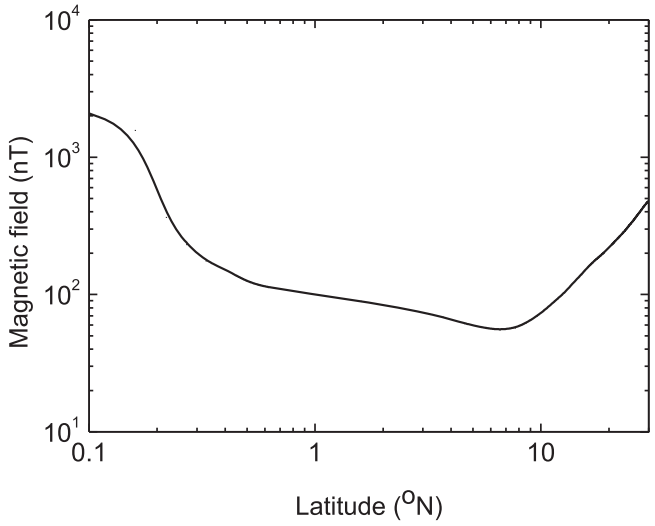

Figure 1. Magnetic field (B_o) along the field line connecting Ganymede and Jupiter is shown as a function of latitude.

2.2. Loss-cone Angle

The magnetic field of the Ganymede–Jupiter system is calculated from

$$\boldsymbol{B} = -\nabla V + \boldsymbol{b} + \boldsymbol{b}_G. \quad (7)$$

The magnetic field of Jupiter is a sum of contributions from internal and external sources. The internal field is derivable from a scalar potential V. We have used the VIP4 model (Connerney et al. 1998) in which V is expressed as a spherical harmonic expansion to degree and order 4. External field $\boldsymbol{b}$ is due to a thin disc-shaped azimuthal current sheet. It is calculated using the analytical expressions given by Connerney et al. (1981, 1982) and Acuna et al. (1983). The component $\boldsymbol{b}_G$ is the magnetic field of Ganymede which is modeled by a Ganymede-centered dipole with dipole moment 1.4×10^{13} Tm^3. Ganymede's magnetic pole is tilted 4° from the spin axis and points toward 156° W in the north and 336° W in the south (Kivelson et al. 2002). The field line connecting Ganymede and Jupiter is traced (Tripathi et al. 2013a, 2014a). In Figure 1 we present the magnetic field on the field line as a function of Jupiter latitude. There are two mirror points on this field line, one near Ganymede and the other near Jupiter. The minimum magnetic field on the field line defines the magnetic equator. The Ganymede side loss-cone is calculated from

$$\mathrm{Sin}^2\,\boldsymbol{\alpha}_{\mathrm{LC}} = \boldsymbol{B}_{\mathrm{eq}}/\boldsymbol{B}_A \quad (8)$$

where B_{eq} is the field at the magnetic equator and B_{A} is the field at the top of the atmosphere of Ganymede, assumed at 1 R_{G} (R_{G} is the radius of Ganymede). Loss-cone angles $\alpha_{\mathrm{LC}} \approx 10.^{\circ}8$–$13.^{\circ}6$ are obtained. Variations of α_{LC} with Ganymede latitude and longitude are not too significant. The separatrix is found near the latitude of 30°.

2.3. Bounce-averaged Diffusion Coefficients

Pitch-angle diffusion coefficients for ECH waves, in units of per second, are given as (Lyons 1974a; Tripathi & Singhal 2009)

$$D_{\alpha\alpha} = \sum_{n=-\infty}^{\infty} \int k_\perp dk_\perp \left[\psi_{n,k} \left(\frac{(n\Omega_e/\omega_k) - \sin^2\alpha}{\sin\alpha\cos\alpha} \right)^2 \right]_{k_\parallel = k_{\mathrm{res}}}, \quad (9)$$

where

$$\psi_{n,k} = \frac{e^2}{4\pi\, m_e{}^2} \frac{|E_k|^2}{V} \left(\frac{\omega_k}{|k|} \right)^2 \frac{J_n{}^2(k_\perp v_\perp/\Omega_e)}{v^4\,|v_\parallel - \partial\omega_k/\partial k_\parallel|}$$

$k_\perp$ and $k_\parallel$ are the components of the wave vector perpendicular and parallel to the ambient magnetic field B_o, respectively, $k_{\mathrm{res}} = (\omega_k - n\Omega_e)/v_\parallel$ is the resonant parallel wave number, $\Omega_e = |eB_o/m_e|$ is the (angular) electron gyrofrequency, ω_k is the wave frequency as a function of k, E_k is the wave electric field at each k, and α and v are the particle pitch angle and velocity, respectively. V is plasma volume, e/m_e is the electron charge to mass ratio, and J_n is the Bessel function of order n. Wave electric field E_k is expressed in the form (Lyons 1974b)

$$|E_k|^2 = [V/N(\omega)]E^2(\omega)g_\omega(\psi) \quad (10)$$

where $E^2(\omega)$ is the wave electric field intensity squared per unit frequency, and $g_\omega(\psi)$ gives the variation of wave electric field energy with wave normal angle for each frequency. We parameterize the wave distribution as follows:

$$E^2(\omega) = E^2_{\mathrm{wave}} \frac{f(\omega)}{\int f(\omega)d\omega} \quad (11)$$

and

$$g_\omega(\psi) = \exp\,[-((x - x_o)/x_\omega)^2]. \quad (12)$$

Here, $x = \cos\psi$, ψ is the wave normal angle (the angle between B_o and k), and $x_o = \cos 89^{\circ}$. The parameter x_ω determines the angular width of the wave electric field energy. It is set equal to 0.01 and assumed independent of the wave frequency. The function $f(\omega)$ determines the distribution of wave energy with wave frequency.

ECH waves can also play a role of heating and accelerating ambient electrons besides pitch-angle scattering. We have, therefore, also calculated momentum diffusion coefficients using

$$D_{\mathrm{pp}} = D_{\alpha\alpha} \left[\frac{\sin\alpha\cos\alpha}{(n\,\Omega_e/\omega_k) - \sin^2\alpha} \right]^2. \quad (13)$$

Bounce-averaged diffusion coefficients are obtained by (Lyons et al. 1972)

$$\langle D_{\alpha\alpha} \rangle = \frac{1}{\tau_B} \int_0^{\tau_B} D_{\alpha\alpha} \left(\frac{\partial\alpha_o}{\partial\alpha} \right)^2 dt \quad (14)$$

and

$$\langle D_{\mathrm{pp}} \rangle = \frac{1}{\tau_B} \int_0^{\tau_B} D_{\mathrm{pp}}\, dt, \quad (15)$$

where α_o is the equatorial pitch angle.

Since ECH waves are generally confined to within a few degrees ($\lambda_{\mathrm{int}} \approx \pm 3^{\circ}$) of the magnetic equator (Gough et al. 1979; Kurth et al. 1980), pitch-angle diffusion is effectively zero outside this latitude range. Assuming that the

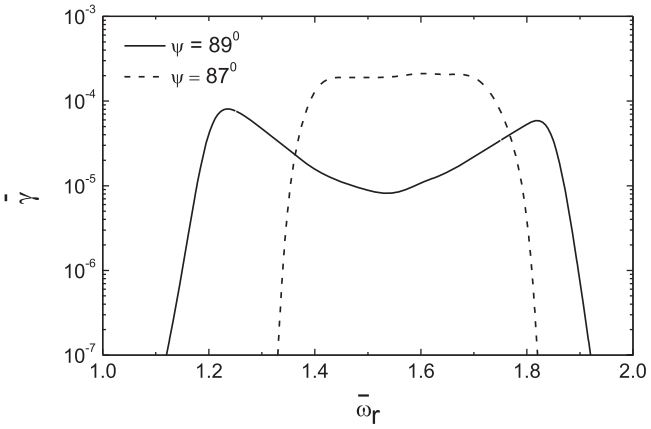

Figure 2. Normalized temporal growth rate $\overline{\gamma}$ ($=\gamma/\Omega_c$) vs. normalized frequency $\overline{\omega}_r$ ($=\omega_r/\Omega_c$). The wave normal angle ψ (angle between wave vector $\boldsymbol{k}$ and ambient magnetic field) is marked.

local diffusion coefficient is approximately constant over this narrow latitude region and neglecting any variations due to changes in pitch angle, we can approximate (Horne & Thorne 2000)

$$\langle D_{\alpha\alpha}\rangle \approx \frac{D_{\alpha\alpha}}{\tau_B}\int_{-\lambda_{\rm int}}^{\lambda_{\rm int}}\frac{2}{v\,\cos\alpha_{\rm o}}\,ds = T_{\rm frac}\,D_{\alpha\alpha}, \quad (16)$$

where

$$T_{\rm frac} = 4\,L\,R_J\,\lambda_{\rm int}/v\cos\alpha_{\rm o}\,\tau_B \quad (17)$$

is the fraction of time the particle interacts with the wave during one bounce period. $D_{\alpha\alpha}$ is evaluated at the magnetic equator. $T_{\rm frac}$ is set equal to 1 for particles with mirror point less than $\lambda_{\rm int}$. Similarly we obtain

$$\langle D_{\rm pp}\rangle = T_{\rm frac}\,D_{\rm pp}. \quad (18)$$

In the Jupiter-centered coordinate system, the location of the magnetic equator is obtained as: radial distance = 15.97 R_J, co-latitude = 83.°4 and west longitude = 289.°5. Plasma parameters at the magnetic equator are: $n_c = 12.5\,{\rm cm}^{-3}$, $T_C =$ 18.6 eV. Equatorial magnetic field is 55 nT. The plasma parameters have been calculated using the model presented by Divine & Garrett (1983). We have used the temporal growth rates of ECH waves to represent the wave frequency spectrum (Tripathi et al. 2013b). It is assumed that wave energy is proportional to the linear temporal growth rate. The linear temporal growth rate profiles, therefore, represent the distribution of wave energy with frequency. Temporal growth rates are calculated using the dispersion relation for electrostatic modes. The electron distribution function, which is a combination of Maxwellian and kappa-loss-cone distribution, is used (Tripathi et al. 2014b). Temporal growth rate profiles are shown in Figure 2. ECH waves are assumed to have a latitudinal extent of $\pm 3°$ from the magnetic equator. The bounce-averaged pitch angle and momentum diffusion coefficients $\langle D_{\alpha\alpha}\rangle$ and $\langle D_{\rm pp}\rangle$ are shown in Figures 3 and 4, respectively, at three representative electron energies 50, 500, and 2 keV. The temporal growth rate profile for wave normal angle $\psi = 89°$ (Figure 2) and ECH wave amplitude 1 mV m^{-1} are used.

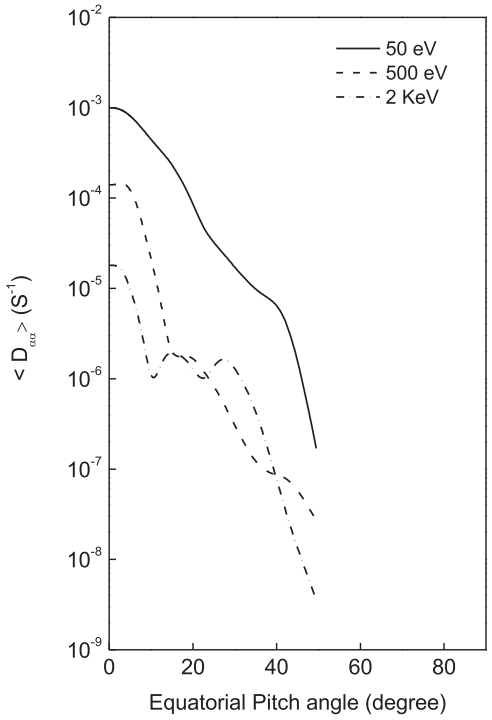

Figure 3. Bounce-averaged electron pitch-angle diffusion coefficients vs. equatorial pitch angle using the temporal growth rate profile from Figure 2 ($\psi = 89°$) for various electron energies. ECH wave amplitude 1 mV m^{-1} is taken.

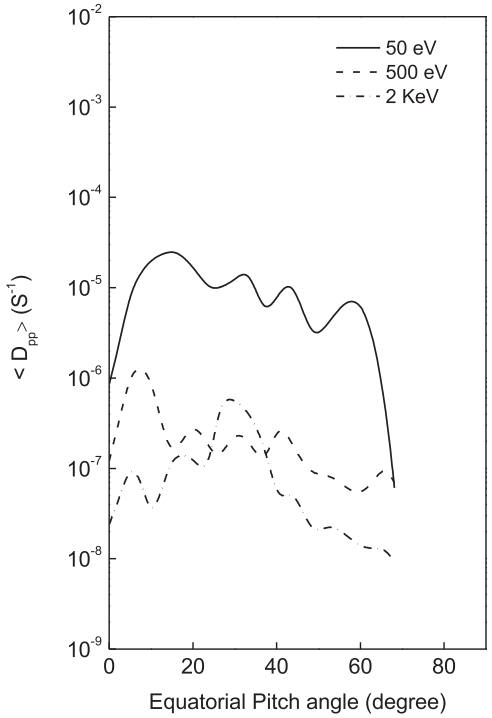

Figure 4. Bounce-averaged momentum diffusion coefficients vs. equatorial pitch angle using the temporal growth rate profile from Figure 2 ($\psi = 89°$) for various electron energies. ECH wave amplitude 1 mV m^{-1} is considered.

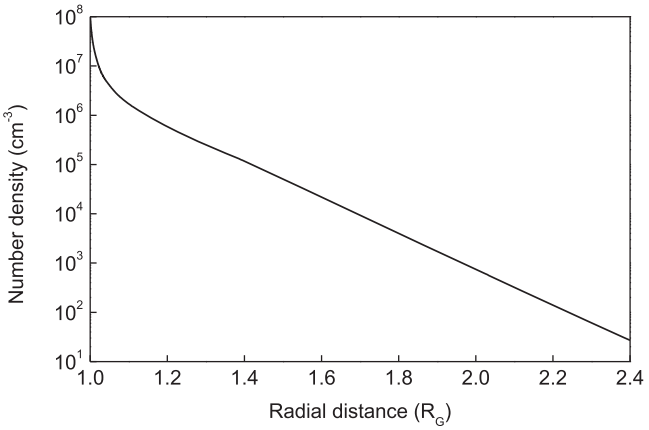

Figure 5. Variation of O_2 number density.

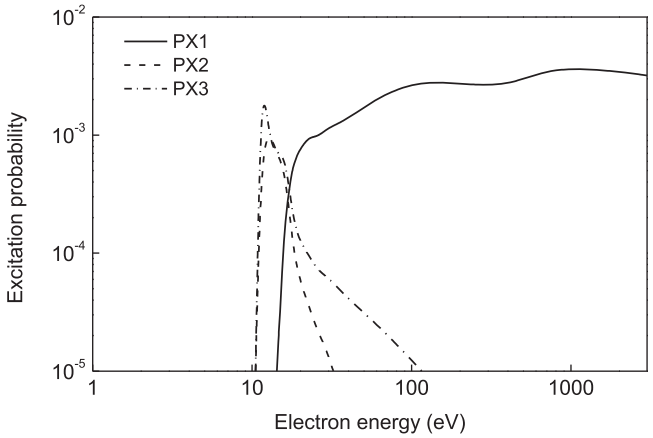

Figure 6. Excitation probability vs. electron energy. PX1 is for dissociative excitation of O_2, PX2 is for excitation of atomic O, PX3 is for cascading.

2.4. Electron Energy Deposition in the Atmosphere of Ganymede

Electron flux precipitated in the atmosphere of Ganymede is used to calculate the emission intensity of O I λ1356 Å. We use the model neutral O_2 atmosphere computed by Eviatar et al. (2001). The model O_2 profile is presented in Figure 5. We have also included atomic oxygen with a constant mixing ratio of 10%. Radial distance from the center of Ganymede is expressed in Ganymede radii (1 R_G = 2634 km). Surface O_2 density is $1 \times 10^8\,\mathrm{cm}^{-3}$ and vertical column density is $2.9 \times 10^{14}\,\mathrm{cm}^{-2}$.

The O I λ1356 Å line is emitted from the transition ($2s^2\,2p^4\ ^3P \leftarrow 2s^2\,2p^3\,3s\ ^5s^0$). We consider following three processes for excitation:

(i) dissociative excitation of O_2 with excitation probability

$$\mathrm{PX1} = \frac{\sigma_d}{\sigma_1 + 0.1\,\sigma_2}; \tag{19}$$

(ii) direct excitation of atomic O with excitation probability

$$\mathrm{PX2} = \frac{0.1\sigma(^5s^0)}{\sigma_1 + 0.1\,\sigma_2}; \tag{20}$$

(iii) direct excitation of atomic O to ($^4s^0$) 3p ^5P followed by cascading to ($^4s^0$) 3s $^5s^0$ with excitation probability

$$\mathrm{PX3} = \frac{0.1\sigma(^5P)}{\sigma_1 + 0.1\,\sigma_2}. \tag{21}$$

σ_1 is the total inelastic electron impact cross section of O_2 and σ_2 is the total inelastic cross section of atomic O. The cross section for dissociative excitation of O_2 (σ_d) is taken from the works of Wells et al. (1971), Erdman & Zipf (1987) and Itikawa et al. (1989). Inelastic cross sections for O_2 and atomic O are taken from the work of Jackman et al. (1977). Calculated excitation probabilities PX1, PX2, and PX3 are presented in Figure 6.

We have calculated the volume excitation rates (VERs) from energy loss of precipitated electrons in the atmosphere of Ganymede. The analytical yield spectrum (AYS) approach for electron energy degradation is used (Green & Singhal 1979; Singhal et al. 1980; Singhal & Green 1981). The AYS approach is described in the Appendix. VER is expressed as

$$\mathrm{VER} = 2\pi \int_{E_1}^{E_2} dE_o \int_0^{\pi/2} d\theta_o \int_{W_{ki}}^{E_o} dE\, J(E_o, \alpha(\theta_o)) \times \sin\theta_o \cos\theta_o\, U(E, Z', E_o)\,\rho(Z)\,p_{ki}(E), \tag{22}$$

where $Z' = Z/\cos\theta_o$.

Here Z is the penetration depth in gm cm^{-2}, U is the AYS, ρ is the atmospheric mass density, and p_{ki} is the excitation probability given by Equations (19)–(21). Integration of Equation (22) over altitude gives the intensity (R), where (1 $R = 10^6$ photons cm^{-2} s^{-1}). It is assumed that each excitation results in the emission of a photon.

For the calculation of precipitation flux J (E_o, $\alpha(\theta_o)$) we require the flux at the edge of the loss-cone J (E_o, α_{LC}). We have considered three cases:

Case A: Magnetospheric electron flux

The flux observed near Ganymede (Frank et al. 1997; Paranicas et al. 1999) is expressed as

$$J(E_o) = \frac{a}{E_o^b} \qquad \text{in units of } (\mathrm{cm^2\ s\ sr\ eV})^{-1}, \tag{23}$$

assuming the flux is isotropic. The parameter details are given in Table 1. Flux below 1 keV has been extrapolated.

We next consider that the ambient electrons near the magnetic equator are being heated and accelerated by the ECH wave turbulence. The Maxwellian (f_M) and kappa (f_κ) distribution functions are used here.

Case B: Maxwellian distribution

$$f_M = \frac{n_h}{\pi^{3/2}\,v_h^3} \exp(-v^2/v_h^2)$$
$$v_h = (2\,T_c/m)^{1/2}$$
$$n_h = 12.5\ \mathrm{cm}^{-3} \text{ is used.} \tag{24}$$

Case C: Kappa distribution

$$f_\kappa = n_h \left(\frac{m}{2\pi\,E_c}\right)^{3/2} \frac{\Gamma(\kappa+1)}{\kappa^{3/2}\,\Gamma(\kappa-1/2)} \frac{1}{\left(1+\frac{E}{\kappa\,E_c}\right)^{\kappa+1}} \tag{25}$$

E_c is the characteristic energy. $\kappa = 2$ and $n_h = 12.5\,\mathrm{cm}^{-3}$ are used. Electron flux is obtained using $J = 2\,Ef/m^2$, m is the mass of an electron.

Table 1
Parameters for Magnetospheric Electron Flux (Case A—Equation (23))

Electron Component	a	b	E_{av} (eV)	N_e (cm^{-3})	Energy Flux (erg cm^{-2} s^{-1})
Thermal (9–100 eV)	1.1×10^{12}	3.52	14.3	100.3	0.50
Suprathermal (100 eV–3 keV)	1.6×10^{7}	1.10	784.3	0.31	0.47

3. RESULTS AND DISCUSSION

In Figure 1 we have presented the magnetic field on the field line connecting Ganymede and Jupiter. It is seen that the magnetic equator is located at 6.6°N Jupiter latitude. In temporal growth rate profiles of ECH waves presented in Figure 2 we note that for wave normal angle $\psi = 89°$, a wider range of normalized frequency ϖ_r (1.20–1.85) is obtained. But the case $\psi = 87°$ yields a narrow range (1.40–1.75) of frequencies. Bounce-averaged pitch-angle diffusion coefficients $\langle D_{\alpha\alpha}\rangle$ for ECH waves at $\psi = 89°$ are depicted in Figure 3. It is evident from Figure 3 that coefficients $\langle D_{\alpha\alpha}\rangle$ cover a narrow range of pitch angles. Further, coefficients $\langle D_{\alpha\alpha}\rangle$ are decreased as the electron energy is increased. It is also noticed that coefficients $\langle D_{\alpha\alpha}\rangle$ for the case of $\psi = 87°$ (not shown) are negligible for energies less than 100 eV. In Figure 4 we show the bounce-averaged momentum diffusion coefficients $\langle D_{pp}\rangle$. It is seen that coefficients $\langle D_{pp}\rangle$ are lower by one to two orders of magnitude in comparison with $\langle D_{\alpha\alpha}\rangle$ coefficients. It is also noted that in general coefficients $\langle D_{pp}\rangle$ cover a wider range of pitch angles and show an oscillatory behavior. The profile of O_2 presented in Figure 5 represents a vertical column density of 2.9×10^{14} cm^2. This is consistent with values used in previous works (Eviatar et al. 2001).

For the emission of O I λ1356 Å, we consider three processes: dissociative excitation of O_2, excitation from atomic O, and cascading. Excitation probabilities for these processes are presented in Figure 6 as a function of electron energy. It is noted that dissociative excitation probability remains significant even at higher energies. As the electron energy increases, the total inelastic cross section of O_2 also decreases. The other two excitation probabilities contribute for energies less than a few tens of eV since the excitation cross section of atomic O states decreases very fast as compared to the total inelastic cross section of O and O_2 at higher electron energies.

Intensities of O I λ1356 Å calculated due to precipitation of magnetospheric electrons (case A, Equation (23)) are presented in Table 2. It is seen from Table 2 that intensities are obtained in the range 8–35 (R). These values are in agreement with other works (Eviatar et al. 2001). The calculated intensities are insufficient to explain the observed diffuse auroral intensities. As noted in previous works, some mechanism to accelerate the electrons is required (Eviatar et al. 2001; Lavrukhin & Alexeev 2015).

Electrostatic ECH wave turbulence may heat and accelerate the ambient electrons near the magnetic equator. It is seen from Figure 4 that the momentum diffusion coefficients are appreciable over a broad range of pitch angles. Thus the electrons may undergo substantial change in momentum. Electrons may also be accelerated in direction parallel to the field line. For electrostatic waves the wave normal is nearly perpendicular to the field lines, thus resulting in increased parallel phase velocity. As a consequence, an electron trapped in the wave may experience a significant increase in velocity as it accelerates to keep up with the parallel component of the phase velocity. For an incoherent wave field, the result will be

Table 2
Calculated Intensities of O I 1356 Å in Rayleigh due to Magnetospheric Electrons (Case A—Equation (23))

Electron Component	1	2	3	4	5
Thermal	6.1	6.0	6.1	16.0	16.0
Suprathermal	6.1	2.3	4.0	12.0	18.8

Notes. (1) Using magnetospheric electron flux, O_2 column density 2.9×10^{14} cm^2. (2) Using precipitation flux, ($\psi = 89°$), ECH wave amplitude 1 mV m^{-1}, O_2 column density 2.9×10^{14} cm^2. (3) Using precipitation flux, ($\psi = 89°$), ECH wave amplitude 3 mV m^{-1}, O_2 column density 2.9×10^{14} cm^2. (4) Using precipitation flux, ($\psi = 89°$), ECH wave amplitude 3 mV m^{-1}, O_2 column density 1.0×10^{15} cm^2. (5) Using magnetospheric electron flux, O_2 column density 1.0×10^{15} cm^2.

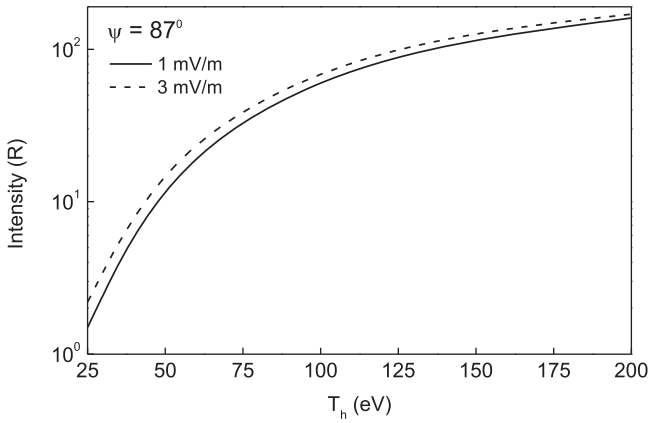

Figure 7. Emission O I 1356 Å intensity in Rayleigh (R) vs. electron temperature (T_h) for a Maxwellian distribution (case B, Equation (24)) using temporal growth rate profiles shown in Figure 2 at $\psi = 87°$.

the production of a beam with a broad energy spectrum (Swift 1970). The accelerated electrons will be subject to a frictional force in the ambient electron gas (Mantas 1975),

$$\frac{dE}{ds} = -\frac{\beta N_e}{E} \tag{26}$$

where $\beta = 2.59 \times 10^{-12}$ (eV^2 cm^2), N_e is electron density, E is the electron energy, and ds is the element of path length. The ambient electron gas may be heated in the process.

We have therefore considered precipitation flux of Maxwellian (case B, Equation (24)) and kappa (case C, Equation (25)) distributions.The intensities due to a Maxwellian distribution as function of thermal temperature are depicted in Figures 7 and 8 for the growth rate profiles (Figure 2) at $\psi = 87°$ and 89°, respectively. The O I λ1356 Å intensities up to ≈150 (R) or higher may be obtained. However, these values are strongly dependent on the heating of ambient electrons by ECH wave turbulence. The values also depend on the amplitude of ECH waves. Higher amplitudes produce higher intensities since $\langle D_{\alpha\alpha}\rangle$ coefficients scale as the square of ECH wave amplitude. The intensities due to a kappa distribution (case C, Equation (25)) are shown in Figures 9 and 10 for the temporal

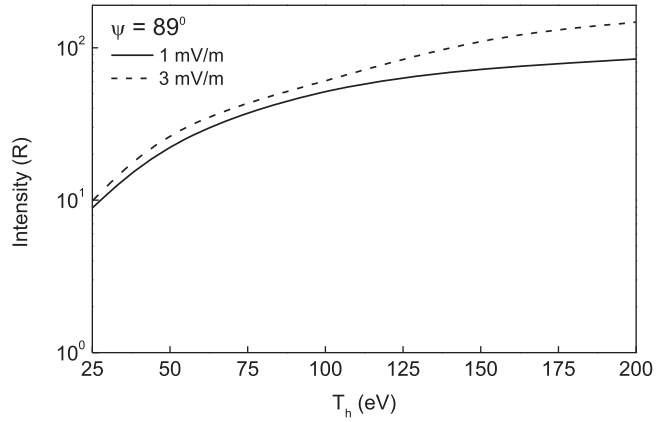

Figure 8. Same as in Figure 7 but using a temporal growth rate profile at $\psi = 89°$.

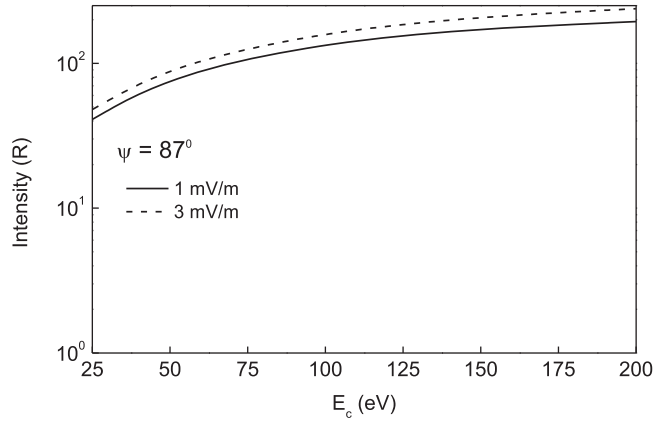

Figure 9. Emission O I 1356 Å intensity in Rayleigh (R) vs. electron characteristic energy (E_c) for a kappa distribution (case C, Equation (25)) using temporal growth rate profiles shown in Figure 2 at $\psi = 87°$.

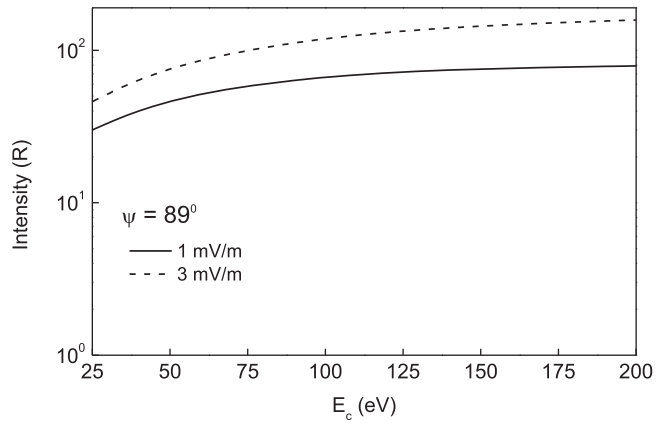

Figure 10. Same as in Figure 9 but using a temporal growth rate profile at $\psi = 89°$.

growth rate profile at $\psi = 87°$ and 89°, respectively. It appears that intensities up to 200 R may be obtained depending on the characteristic energy. It is also found from Figures 7–10 that intensities for the case $\psi = 87°$ are generally higher than the intensities calculated for $\psi = 89°$. This may be understood from the temporal growth rate profiles for $\psi = 87°$ and 89° shown in Figure 2. The profile for $\psi = 87°$ produces larger wave growth rates as compared to that for $\psi = 89°$. This results in larger pitch-angle diffusion coefficients for $\psi = 87°$ and

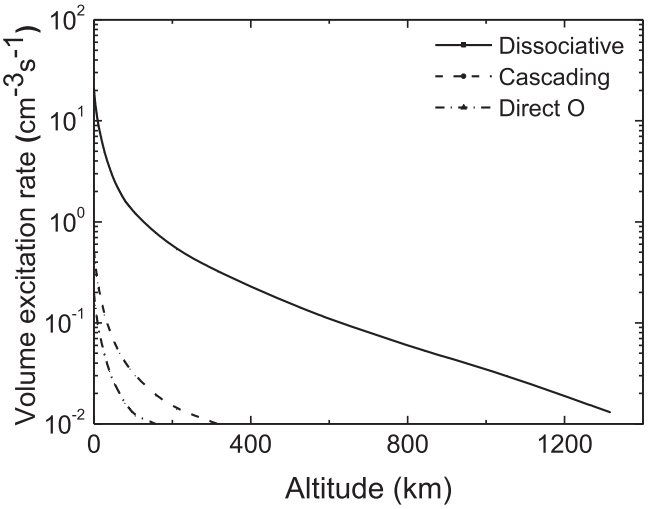

Figure 11. Volume excitation rate (VER) vs. altitude profiles for dissociative excitation, direct atomic O, and cascading contribution as marked. Maxwellian distribution, temporal growth rate for $\psi = 87°$, ECH wave amplitude 1 mV m^{-1}, and $T_h = 100$ eV are used.

hence a larger precipitation flux into the loss-cone. Further, it is seen that in general higher intensities are obtained from a kappa distribution as compared to those for a Maxwellian distribution. The reason for this lies in the fact that a kappa distribution function has a high energy tail whereas the Maxwellian distribution falls off much more rapidly with increasing energy. Therefore, the contribution to VER from a kappa distribution function is higher than that from a Maxwellian distribution. Acceleration of ambient electrons by electrostatic ECH wave turbulence may produce a high energy tail and a Maxwellian distribution is appropriate for heating by electrostatic waves.

Finally in Figure 11 we present the VER as a function of altitude for a representative case: $\psi = 87°$, Maxwellian distribution with $T_h = 100$ eV and ECH wave amplitude 1 mV m^{-1}. It is seen that most of the electron energy is deposited within about 200 km from the surface of Ganymede. The major contribution to VER appears from dissociative excitation of O_2. Contributions from direct atomic O excitation and cascading are quite small. Emission O I λ1356 Å intensities for three processes: dissociative, direct O, and cascading are 66.6 R, 0.65 R, and 1.7 R, respectively.

In the present work we have dealt with the role of ECH waves in generating diffuse aurora on Ganymede. However, whistler mode waves are also observed near Ganymede. Whistler mode waves would also contribute to the diffuse auroral precipitation on Ganymede. Whistler mode chorus has been understood as the dominant trigger to the diffuse aurora at Earth (Thorne et al. 2010; Ni et al. 2011, 2014). These waves generally resonate with electrons of higher energy as compared to the electrons energies resonating with ECH waves. In ECH waves, use of a Maxwellian distribution with temperature 100 eV produces about 50–70 R of emission O I 1356 Å intensities. In the case of whistler mode waves it would require somewhat higher temperature ≈150 eV to produce intensities of similar magnitude. A detailed and comprehensive study of diffuse aurora on Ganymede due to whistler mode waves has just been submitted (Tripathi et al. 2016).

Electron density on the magnetic equator on the field line connecting the north pole of Ganymede to Jupiter is 12.5 cm^{-3} and on the field line connecting the south pole of Ganymede to

Jupiter, the value is 7 cm^{-3} (Divine & Garrett 1983). The diffuse auroral emissions in the southern hemisphere of Ganymede should therefore be lower as compared to intensities in the northern hemisphere (Hall et al. 1998).

4. CONCLUSIONS

The role of electrostatic ECH waves in producing the diffuse O I 1356 Å emissions on Ganymede is studied. Electron precipitation flux entering the atmosphere of Ganymede due to pitch-angle diffusion into the loss-cone by ECH waves has been estimated. The AYS approach for electron energy degradation has been used to calculate diffuse auroral intensities. The effect of the ECH wave spectral intensity profile and ECH wave amplitude on calculated intensities has been studied. The heating and acceleration of ambient electrons by ECH wave turbulence at the magnetic equator is modeled by using Maxwellian and kappa electron distribution functions. The main results of the present study may be summarized as follows:

1. Intensities of O I 1356 Å emissions calculated due to the precipitation of magnetospheric electrons observed near Ganymede are found too small to account for the observed diffuse emissions. This is in agreement with conclusions reached in previous works (Eviatar et al. 2001).
2. Use of a Maxwellian distribution function to model heating and acceleration of ambient electrons by ECH wave turbulence can produce intensities ≈50–70 R for a temperature of 100 eV.
3. Use of a kappa distribution function with characteristic energy 50 eV can also produce intensities ≈50–80 R.
4. The spectral intensity profile and ECH wave amplitude have very significant effects on calculated intensities.
5. The calculated intensities strongly depend on ambient electron density, and temperature/characteristic energy of the electron distribution function. Further, it is seen that the use of a kappa distribution function to simulate heating/acceleration of ambient electrons produces in general higher intensities as compared to those from a Maxwellian distribution. Future joint NASA/ESA *Jupiter Icy Moons Explorer* and *JUNO* missions to Jupiter may provide new data to confirm the findings of the present study.

This work was supported by the Planetary Sciences and Exploration Programme, Indian Space Research Organization (ISRO), PRL, Ahmedabad under the sanctioned project scheme. Calculations reported in the present work were carried out at the Computer Centre, Banaras Hindu University.

APPENDIX
ANALYTICAL YIELD SPECTRUM

Energy degradation of monoenergetic electrons in planetary atmospheric gases has been studied using a Monte Carlo technique (Green & Singhal 1979; Singhal et al. 1980; Singhal & Green 1981). A function which has been called "yield spectra" is obtained from the Monte Carlo simulation. The three-dimensional yield spectra $U(E, Z, E_o)$ is defined as

$$U\ (E, Z, E_o) = \frac{N\ (E, Z)}{\Delta E\ \Delta Z}\ (\mathrm{eV})^{-1}\ \ (\mathrm{gm\ cm^{-2}})^{-1}, \qquad (27)$$

where $N\ (E, Z)$ is the total number of inelastic collisions that exist in the spatial interval ΔZ around Z, in the energy interval ΔE centered at E after the incident electron energy of energy E_o and all its secondaries, tertiaries, etc. have been completely degraded in energy. The numerical yield spectral function generated by Monte Carlo simulation is represented analytically

$$U\ (E, Z, E_o) = \sum_{i=0}^{2} \frac{A_i'}{R}\ \chi^i\ G_i(Z), \qquad (28)$$

where $\chi = \frac{E_k^{\Omega}}{E+L}$, $E_k = \frac{E_o(\mathrm{eV})}{1000}$, $L = 1$ eV, $\Omega = 0.585$.

G_i is a microplume of the form

$$G_i = \exp\ \lfloor -\beta_i^2\ Z^2 + \gamma_i\ Z \rfloor. \qquad (29)$$

Z is longitudinal distance expressed in fraction of a scale factor R (in gm cm^{-2}). β_i, γ_i, A_i' depend on E_o. It is found that the AYS function where distances are expressed in gm cm^{-2} has almost a universal character.

REFERENCES

Acuna, M. H., Behannon, K. W., & Connerney, J. E. P. 1983, in Physics of the Jovian Magnetosphere, ed. A. Dessler (New York: Cambridge Univ. Press), 1
Calvin, W. M., Johnson, R. E., & Spencer, J. R. 1996, GeoRL, 23, 673
Chang, H. C. 1983, Space Telecommun and Radiosci Lab, Tech. Rep. E414-1 (Stanford California: Stanford Univ.)
Connerney, J. E. P., Acuna, M. H., & Ness, N. F. 1981, JGR, 86, 8370
Connerney, J. E. P., Acuna, M. H., & Ness, N. F. 1982, JGR, 87, 3623
Connerney, J. E. P., Acuna, M. H., Ness, N. F., & Satoh, T. 1998, JGR, 103, 11929
Divine, N., & Garrett, H. B. 1983, JGR, 88, 6889
Erdman, P. W., & Zipf, E. C. 1987, JChPh, 87, 4540
Eviatar, A., Strobel, D. F., Wolven, B. C., et al. 2001, ApJ, 555, 1013
Feldman, P. D., McGrath, M. A., Strobel, D. F., et al. 2000, ApJ, 535, 1085
Frank, L. A., Paterson, W. R., & Ackerson, K. L. 1997, GeoRL, 24, 2159
Gough, M. P., Christiansen, P. J., Martelli, G., & Gershuny, E. J. 1979, Natur, 279, 515
Green, A. E. S., & Singhal, R. P. 1979, GeoRL, 6, 625
Grundy, W. M., Buratti, B. J., Cheng, A. F., et al. 2007, Sci, 318, 234
Gurnett, D. A., Kurth, W. S., Roux, A., Bolton, S. J., & Kennel, C. F. 1996, Natur, 384, 535
Gurnett, D. A., Kurth, W. S., & Scarf, F. L. 1979, Sci, 206, 987
Hall, D. T., Feldman, P. D., McGrath, M. A., & Strobel, D. F. 1998, ApJ, 499, 475
Horne, R. B., & Thorne, R. M. 2000, JGR, 105, 5391
Itikawa, Y., Ichimura, A., Onda, K., et al. 1989, JPCRD, 18, 23
Jackman, C. H., Garvey, R. H., & Green, A. E. S. 1977, JGR, 82, 5081
Kennel, C. F. 1969, RvGeo, 7, 379
Kennel, C. F., & Petschek, H. E. 1966, JGR, 71, 1
Kivelson, M. G., Khurana, K. K., Coroniti, F. V., et al. 1997, GeoRL, 24, 2155
Kivelson, M. G., Khurana, K. K., Russell, C. T., et al. 1996, Natur, 384, 537
Kivelson, M. G., Khurana, K. K., & Volwerk, M. 2002, Icar, 157, 507
Kurth, W. S., Gurnett, D. A., Roux, A., & Bolton, S. J. 1997, GeoRL, 24, 2167
Kurth, W. S., Gurnett, D. A., & Scarf, F. L. 1980, GeoRL, 7, 61
Lavrukhin, A. S., & Alexeev, I. I. 2015, AstL, 41, 687
Lyons, L. R. 1974a, JGR, 79, 575
Lyons, L. R. 1974b, JPlPh, 12, 417
Lyons, L. R., Thorne, R. M., & Kennel, C. F. 1972, JGR, 77, 3455
Mantas, G. P. 1975, P&SS, 23, 337
McGrath, M. A., Jia, X., Retherford, K., et al. 2013, JGRA, 118, 2043
Mead, G. D. 1974, JGR, 79, 3487
Ni, B., Bortnik, J., Nishimura, Y., et al. 2014, JGRA, 119, 897
Ni, B., Liang, J., Thorne, R. M., et al. 2012, JGR, 117, A01218
Ni, B., Thorne, R. M., Meredith, N. P., Horne, R. B., & Shprits, Y. Y. 2011, JGR, 116, A04219
Ni, B., Thorne, R. M., Zhang, X., et al. 2016, SSRv, 200, 205
Orlova, K. G., & Shprits, Y. Y. 2011, PhPl, 18, 092904
Paranicas, C., Paterson, W. R., Cheng, A. F., et al. 1999, JGR, 104, 17,459
Scarf, F. L., Gurnett, D. A., & Kurth, W. S. 1979, Sci, 204, 991
Scudder, J. D., Sittler, E. C., & Bridge, H. S. 1981, JGR, 86, 8157

Singhal, R. P., & Green, A. E. S. 1981, JGR, 86, 4776
Singhal, R. P., Jackman, C. H., & Green, A. E. S. 1980, JGR, 85, 1246
Susanna, M., Ferenc, V., William, M., & Gerald, S. 2002, Icar, 159, 500
Swift, D. W. 1970, JGR, 75, 6324
Thorne, R. M., Ni, B., Tao, X., Horne, R. B., & Meredith, N. P. 2010, Natur, 467, 943
Tripathi, A. K., & Singhal, R. P. 2009, PhPl, 16, 1
Tripathi, A. K., Singhal, R. P., Singh, K. P., & Singh, O. N., II 2013a, Icar, 225, 424
Tripathi, A. K., Singhal, R. P., Singh, K. P., & Singh, O. N., II 2013b, JASTP, 97, 125
Tripathi, A. K., Singhal, R. P., Singh, K. P., & Singh, O. N., II 2014a, P&SS, 92, 150
Tripathi, A. K., Singhal, R. P., Singh, K. P., & Singh, O. N., II 2014b, Ap&SS, 352, 421
Tripathi, A. K., Singhal, R. P., & Singh, O. N., II 2016, AnGp, submitted
Wells, W. C., Borst, W. L., & Zipf, E. C. 1971, CPL, 12, 288
Williams, D. J., & Mauk, B. 1997, JGR, 102, 24,283
Williams, D. J., Mauk, B., & McEntire, R. W. 1997a, JGR, 103, 17523
Williams, D. J., Mauk, B., & McEntire, R. W. 1997b, GeoRL, 24, 2953
Williams, D. J., McEntire, R. W., Jaskulek, S., & Wilken, B. 1992, SSRv, 60, 385